Publ. Astron. Soc. Japan 33, 665-677 (1981)

Neutral Hydrogen in M 31. II. Kinematical Properties and Density Waves

Takeyasu SAWA

Department of Earth Science, Aichi University of Education, Kariya, Aichi 448

and

Yoshiaki SOFUE*

Department of Physics and Astrophysics, Nagoya University, Chikusa-ku, Nagoya 464

(Received 1981 January 23; revised 1981 June 19 and August 17)

Abstract

The density-wave theory is applied to the neutral hydrogen (H I) data of M31 to calculate model $T(\lambda, v)$ and $T(\beta, v)$ diagrams (the brightness temperature of the 21-cm line emission plotted on the longitude–radial velocity and latitude–radial velocity planes), when the galaxy is observed with a finite antenna beam width. The calculated results reproduce many characteristic features like bifurcated distribution on observed $T(\lambda, v)$ and $T(\beta, v)$ diagrams for H I gas in M31. We further determine positions of spiral arms using the H I line data in a framework of the density-wave theory. Outer H I arms at radii greater than 15 kpc from the center of M31 define a two-armed trailing spiral structure.

Key words: Density waves; Galaxies; M31; Neutral hydrogen; Spiral structure of galaxies.

1. Introduction

Modeling the $T(l, v)$ diagrams (the brightness temperature of the 21-cm line emission plotted on the galactic longitude–radial velocity plane) for our Galaxy based on the density-wave theory provides a useful mean to investigate kinematical properties and the spiral structure of the Galaxy, because the diagrams can be directly compared with observations (e.g., Burton 1971, 1976; Simonson 1976; Sawa 1978). Although a similar method has been needed for external galaxies, insufficient sensitivity and velocity resolution have restricted its application.

However, recent high-sensitivity and high-velocity dispersion observations of the 21-cm line of M31 (Cram et al. 1980) appear to make it possible to model and compare the longitude- and latitude–radial velocity diagrams of the brightness temperature for this external galaxy. The observations were made with an angular resolution of 9′, an rms sensitivity of 50 mK, and a velocity resolution

* Present address: Nobeyama Radio Observatory, Nobeyama, Minami-saku-gun, Nagano 384-13.

of 5.5 km s^{-1}. In this paper we compute the diagrams for M31 on the basis of the density-wave theory of Lin et al. (1969) so that the results can be directly compared with the data of Cram et al. (1980). We further propose a new method to derive spiral-arm positions by use of the diagrams in such a highly inclined galaxy as M31. The method will be complementary to the velocity-to-space transformation method proposed in our previous paper [Sofue and Kato (1981); referred to as Paper I], in which the noncircular motion such as due to density waves was neglected.

2. Density-Wave Theory Applied to M31

In order to calculate line profiles of the 21-cm line emission of the neutral hydrogen in M31, we construct a kinematical model for the distribution and motion of the interstellar gas in M31 based on the linear density-wave theory of Lin et al. (1969). We assume the distance to M31 to be 690 kpc, the inclination of the disk 77°, and the systemic radial velocity of the galaxy −300 km s^{-1}.

2.1. Overall Distribution of the Gas and Rotation Curve

In Paper I, we have shown that the H I gas in M31 has a ring-like distribution. The gas is concentrated in a ring with a width of 8 kpc centered at a radius 12 kpc from the center of the galaxy with a surface density of about 4×10^{20} atoms cm^{-2}. In the following calculations we adopt a radial distribution as shown in figure 1 for the H I gas density, which represents a first approximation to the observed radial distribution. The mean motion of the gas in M31 is assumed to be circular. The rotation curve used in the present paper is shown in figure 2.

2.2. Density-Wave Theory

M31 is a spiral galaxy of Sb type, whose spiral arms may be well represented by the density wave of Lin et al. (1969). Since we do not attempt to construct a self-consistent model, we consider only a response of the gas to the nonaxisymmetric perturbation of the gravitational field due to the background stellar density waves. Then the motion of the gas can be expressed by the superposition of two components, i.e., the axisymmetric circular rotation and the perturbed motion due to the density waves. The response of the gas to a stellar

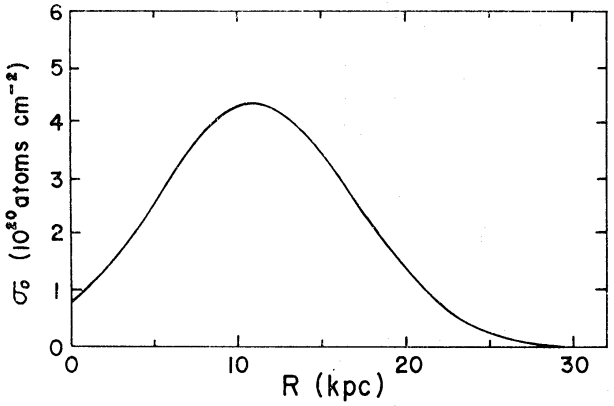

Fig. 1. Mean surface density of H I atoms σ_0 in the disk of M31 assumed for the model computations.

density wave with a small amplitude can be described by the following parameters. Here we assume a two-armed bisymmetric spiral pattern.

Ω_p=angular velocity of the density waves,

F=amplitude of the density waves as a fraction of the axisymmetric gravitational field,

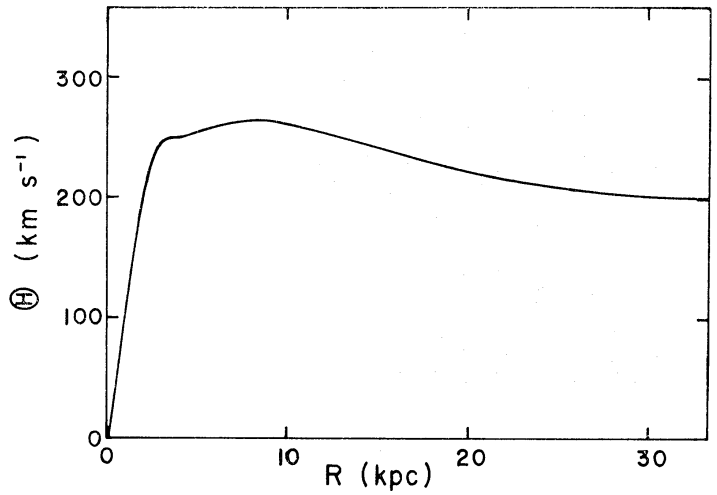

Fig. 2. A smoothed rotation curve of M31 which defines the mean rotation velocity Θ of the disk.

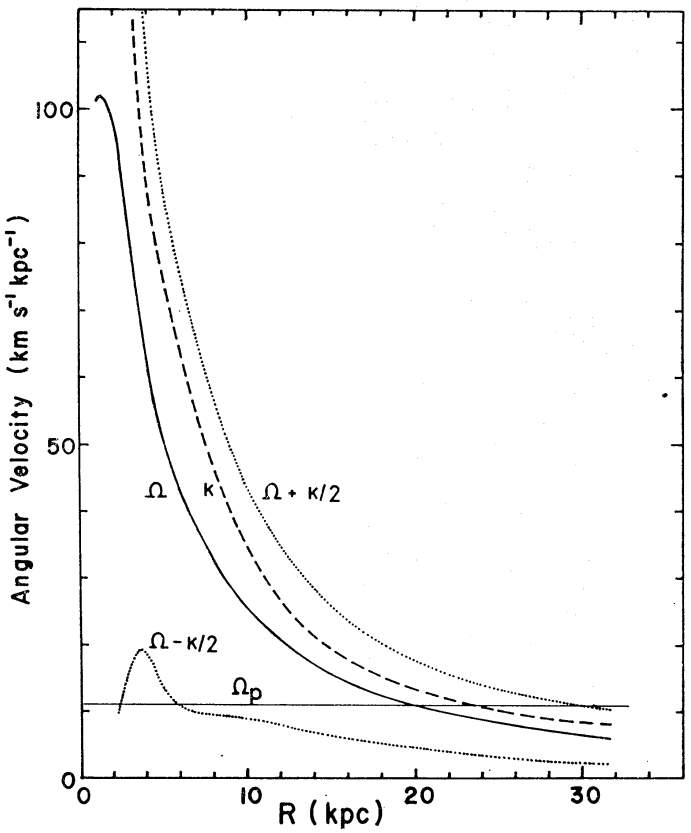

Fig. 3. Kinematical quantities assumed for M31 as functions of radius: Ω= angular velocity of the disk rotation; Ω_p=angular velocity of the density waves; κ=epicyclic frequency.

α=pitch angle of the density-wave pattern.

These parameters are determined by observations. Guibert (1974) has obtained a pattern speed of $\Omega_p=11\,\mathrm{km\,s^{-1}\,kpc^{-1}}$ by fitting the self-consistent density-wave theory to his H I data. Arp (1964) has proposed a two-armed logarithmic spiral with $\alpha=7°.4$. We assume that the amplitude of the stellar density wave is the same as that for our Galaxy, e.g., $F=0.05$ (Yuan 1969). In summary we adopt $\Omega_p=11\,\mathrm{km\,s^{-1}\,kpc^{-1}}$, $F=0.05$, and $\alpha=7°.4$ in this section.

The perturbed surface density σ_1 of the H I gas and its velocity components in the radial and azimuthal directions, u_R and u_ϕ, in the cylindrical coordinate system (R,ϕ,z) are given by

$$\frac{\sigma_1}{\sigma_0}=\frac{\Omega}{\kappa}\frac{2F}{(1-\nu^2+x)\sin\alpha}\cos\chi\,, \tag{1}$$

$$\frac{u_R}{R\Omega}=\frac{\Omega}{\kappa}\frac{F}{(1-\nu^2+x)}\cos\chi\,, \tag{2}$$

$$\frac{u_\phi}{R\Omega}=\frac{F}{2(1-\nu^2+x)}\sin\chi\,, \tag{3}$$

where σ_0 is the mean surface density at R, $\Omega(R)$ is the angular velocity of the circular rotation, and κ is the epicyclic frequency defined by

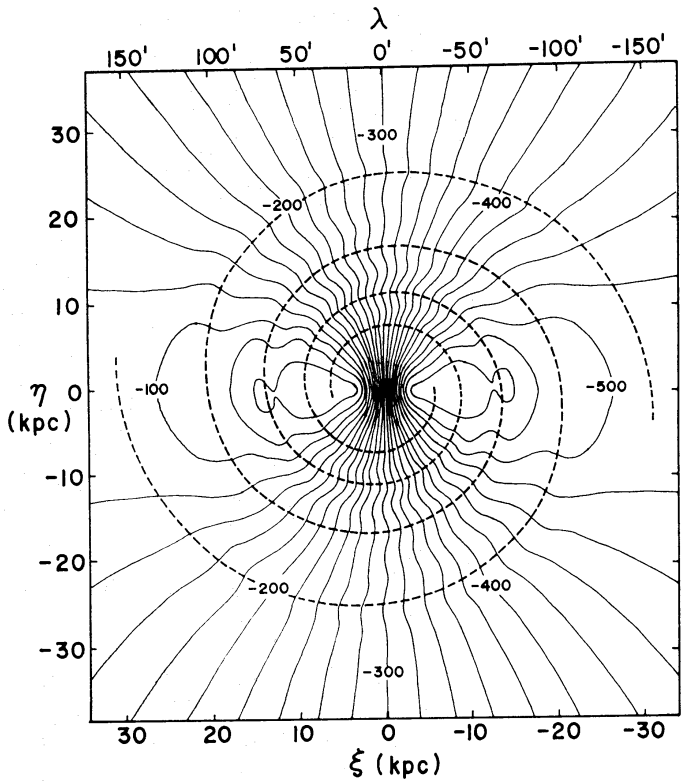

Fig. 4. Radial velocity field of M31 expected from the rotation curve in figure 2 and the density-wave model. The spiral density waves are imposed by the dashed lines. The coordinates ξ and η are rectangular ones on the galaxy plane parallel and perpendicular to the major axis of M31, respectively (see Paper I).

$$\kappa^2=4\Omega^2\left(1+\frac{R}{2\Omega}\frac{d\Omega}{dR}\right). \quad (4)$$

Here χ is the phase angle of the stellar density waves, and ν and x are given by

$$\nu=\frac{2(\Omega_p-\Omega)}{\kappa} \quad (5)$$

and

$$x=\frac{4a^2}{R^2\kappa^2\sin^2\alpha}, \quad (6)$$

where a denotes the mean velocity dispersion of the H I gas, which we take typically as 8 km s^{-1}. Positions of the maximum amplitude of the density waves correspond to $\chi=2n\pi$ ($n=0, \pm1, \pm2, \cdots$). For the constant pitch angle α, the phase angle χ is given by

$$\chi=2\left[\phi-\cot\alpha\ln\left(\frac{R}{R_0}\right)\right]-\chi_0, \quad (7)$$

where R_0 and χ_0 are constants.

Figure 3 shows the rotation parameters for the M31 disk as calculated from the above model. In this model the corotation occurs at $R\sim20$ kpc and the inner and outer Lindblad resonances occur at 6 and 30 kpc, respectively. Figure 4 shows the distribution of the radial velocity calculated from the above model as seen from the sun. The dashed lines in figure 4 indicate the model spirals adopted here, which are identical with those proposed by Arp (1964).

3. $T(\lambda, v)$ and $T(\beta, v)$ Diagrams

On the basis of the density-wave model described in the previous section, we compute velocity profiles (brightness temperature T as a function of radial velocity v) over the M31 disk. To compare the computed results with observations, it is convenient to construct $T(\lambda, v)$ and $T(\beta, v)$ diagrams. Namely, the brightness temperature of the H I line emission plotted on the (λ, v) and (β, v) coordinates in the form of contour diagrams, where λ and β are the rectangular coordinates parallel and perpendicular to the major axis of M31 on the sky, respectively. The readers are referred to Paper I as to the detailed orientation of the galaxy and the definition of the coordinates.

The diagrams are constructed for such a case, where the galaxy is observed with a Gaussian beam elongated in the minor axis with a half-power beam width of 9′. The resolution of 9′, the same as the antenna beam width of the 100-m telescope with which the H I line data by Cram et al. (1980) were obtained. This corresponds to a spatial resolution of 1.8 kpc in the direction of the major axis and 8 kpc in the direction of the minor axis on the plane of the galaxy. A detailed procedure of model making is found in Sawa (1978). Below we discuss the resulting diagrams in comparison with the observations.

3.1. $T(\lambda, v)$ Diagram

Figure 5 shows thus computed $T(\lambda, v)$ diagrams of M31 at three fixed latitudes: $\beta=0'$, $-9'$, and $-18'$. Figure 6 shows the observed $T(\lambda, v)$ diagrams at

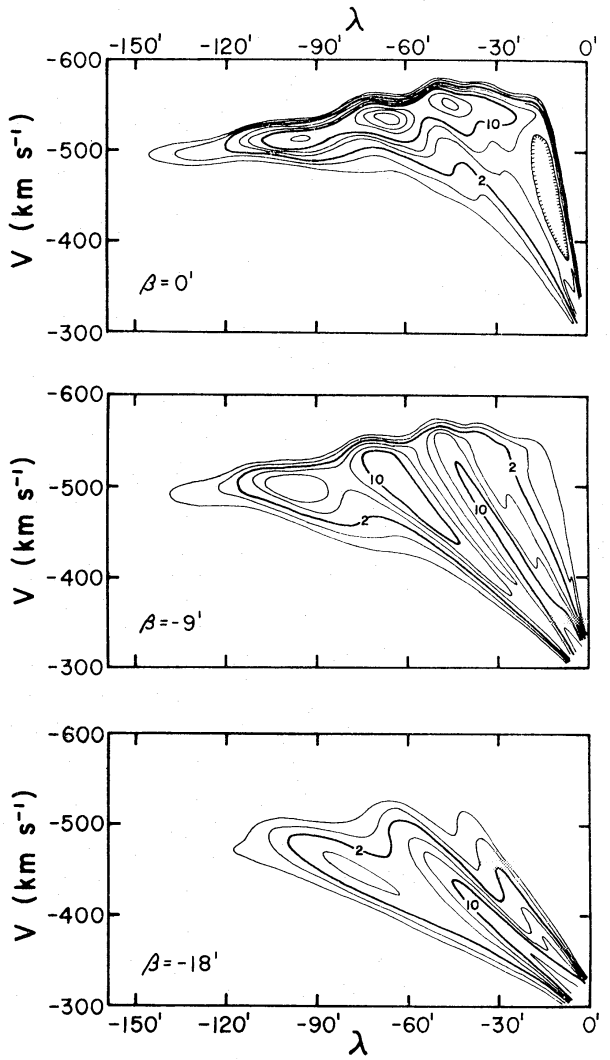

Fig. 5. Calculated $T(\lambda, v)$ diagrams for M31 at $\beta=0'$, $-9'$, and $-18'$. The contour levels are 0.4, 1, 2, 4, 6, 10, 20, 30, and 40 K, respectively. Compare with the observed diagrams in figure 6.

the same latitudes reproduced from Cram et al. (1980). We find a good agreement in general features between the calculated results and the observations. The model diagram at $\beta=0'$ (along the major axis) shows some intensity peaks near the upper edge of the contours at $\lambda=-45'$, $-65'$, and $-95'$ superimposed on a ridge running parallel to the terminal velocity. The wavy variation of the terminal velocity (or the rotation curve) is due to the noncircular motion of the gas caused by the density waves: The gas rotates slower in the inner side of the spiral arm, while it rotates faster in the outer side. These features are in good agreement with the observed diagram at $\beta=0'$, except for the accurate positions of the peaks which appear at $\lambda=-45'$, $-63'$, and $-115'$ in figure 6, a lower value of the radial velocity than the observed values at $\lambda>100'$, and a larger spread in the radial velocity. The lower radial velocity is due to the rotation curve chosen (figure 2). A flatter rotation curve might lead to a better fit to the observation. The observed spread in velocity cannot be explained by the beam-width effect, but is probably due to a warping of the disk of M31 as

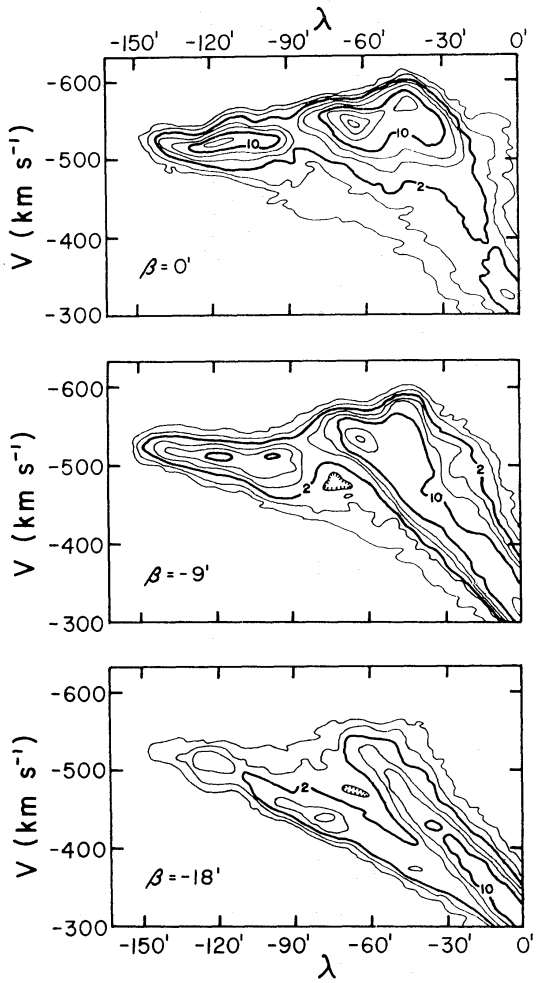

Fig. 6. Observed $T(\lambda, v)$ diagrams for M31 at $\beta=0'$, $-9'$, and $-18'$ reproduced from Cram et al. (1980). The contour levels are the same as those of figure 5.

has been shown by Whitehurst et al. (1978).

The model $T(\lambda, v)$ diagram at $\beta=-9'$ shows features similar to those at $\beta=0'$, but the horizontal ridge and peaks at the terminal velocities become relatively weaker. Instead some inclined ridges become prominent and run from the lower right of the figure towards the upper edge of the contours. These "bifurcated" ridges are due to the spiral condensations and the noncircular motion of the gas caused by the density waves. The bifurcation into three ridges is still observed in the model diagram at $\beta=-18'$, where the ridge corresponding to the outermost arm becomes relatively stronger. The bifurcated features are characteristic of the observed $T(\lambda, v)$ diagram (figure 6).

3.2. $T(\beta, v)$ Diagram

Figure 7 shows the calculated $T(\beta, v)$ diagrams at fixed longitudes: $\lambda=-36'$, $-72'$, and $-90'$. Figure 8 shows the observed diagrams from Cram et al. (1980). The overall features in the model diagrams are symmetric with respect to the line of $\beta=0'$. They are further superimposed by some intensity peaks which do not necessarily appear symmetrically. The asymmetric appearance of the peaks

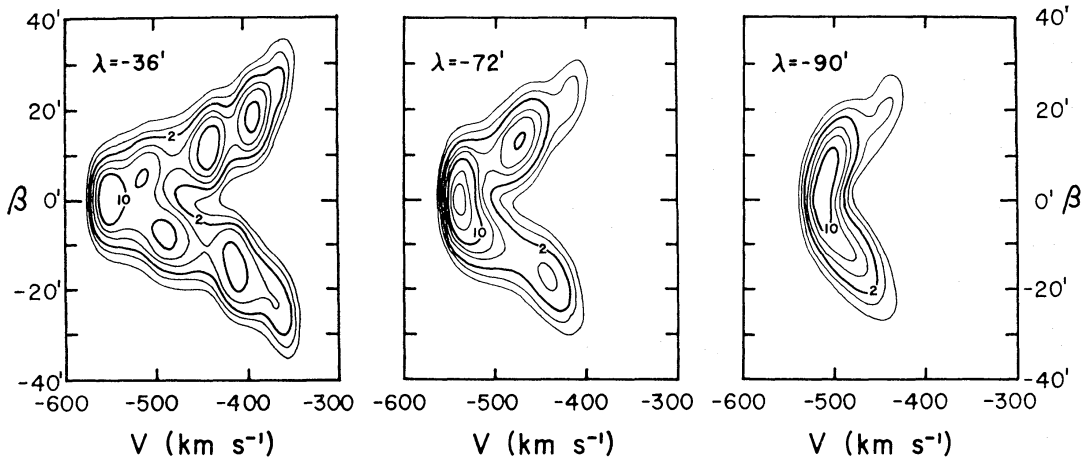

Fig. 7. Calculated $T(\beta, v)$ diagrams for M31 at $\lambda=-36'$, $-72'$, and $-90'$. Compare with the observed diagrams in figure 8.

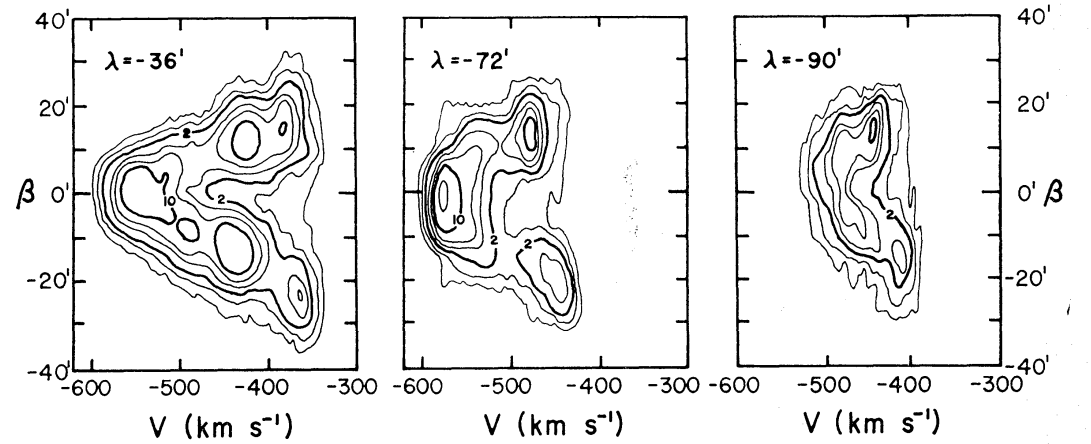

Fig. 8. Observed $T(\beta, v)$ diagrams at $\lambda=-36'$, $-72'$, and $-90'$ reproduced from Cram et al. (1980).

is due to the assumed spiral pattern. The peaks at $\beta\neq 0'$ correspond to intersections of the line of constant λ within the beam and the spiral arms. The peak at $\beta=0'$ is mainly due to the fact that the velocity gradient becomes small and tends to zero at the major axis, i,e., due to the velocity "crowding" in the line of sight at $\beta\sim 0'$. All these features are in fact well observed in the $T(\beta, v)$ diagrams of Cram et al. (1980) reproduced in figure 8.

From a comparison of the calculated results with the observed diagrams (figures 5–8), we may conclude that the density-wave theory can reasonably account for the characteristic features in the $T(\lambda, v)$ and $T(\beta, v)$ diagrams of M31; the intensity peaks and bifurcated ridges in the $T(\lambda, v)$ diagrams and intensity peaks in the $T(\beta, v)$ diagrms are produced by the density-wave spiral arms.

4. Spiral Structure of M31

Although the general characteristics in the $T(\lambda, v)$ and $T(\beta, v)$ diagrams are well understood by our model, we find some disagreement between the positions of the intensity peaks in the observed and calculated diagrams (see figures 5–8).

This is due to our oversimplified spiral shape. The peak and ridge positions strongly depend on the positions of spiral arms and scarcely depend on the other parameters. Using this characteristic, we may be able to find true positions of the arms so that the positions of the peaks and ridges on the $T(\lambda, v)$ and $T(\beta, v)$ diagrams for the model spirals coincide with the observed peak and ridge positions.

It is clear that such a grand design of bisymmetric, simple logarithmic spirals in figure 4 does not fit the entire arms in M31, even if we adjust only either the pitch angle or position angle of the spirals or both. Therefore the fitting is possible only locally by adjusting the model peak position to its nearest observed position of a peak on the diagram. In fact, in the following, we apply such a local adjusting procedure to find true arm positions; we trace the local arm positions, or segments of logarithmic spirals at various position angles, from point to point on the M31 disk to get a set of "arms." Namely, we consider that the arms in M31 are composed of a complex superposition of segments of logarithmic spirals at various position angles but with a constant pitch angle. Then the resulting "arms" will no longer fit the original grand design of bisymmetric spirals; parameters like pitch angles and position angles of "arms" thus obtained may be different from those in the original model spirals. In the following, we describe details of the procedure of local adjusting.

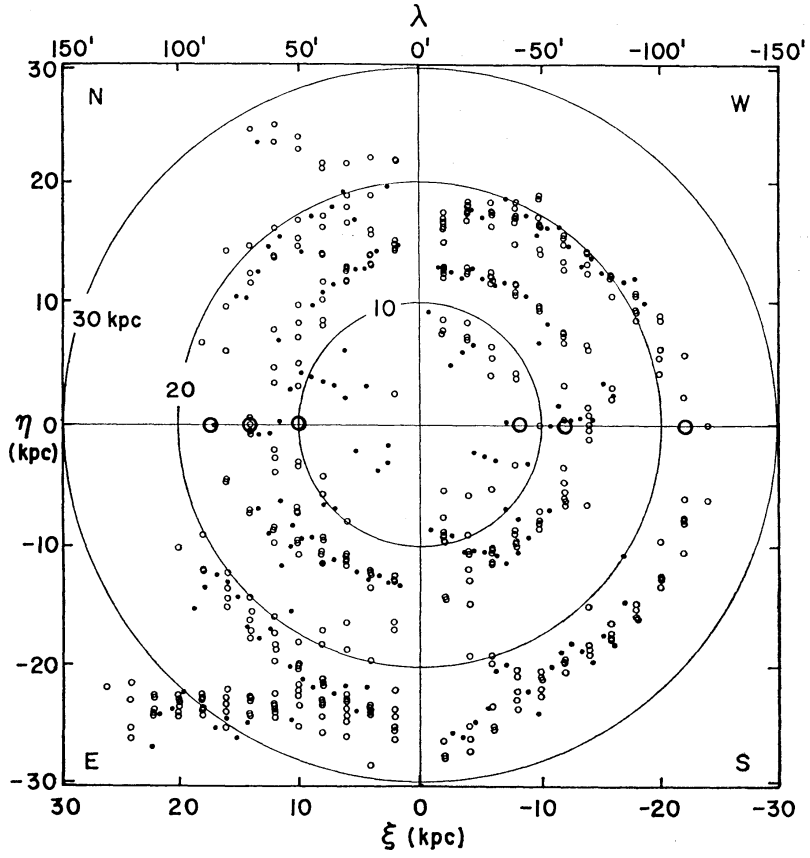

Fig. 9. Positions of ridges on $T(\lambda, v)$ diagrams (open circles) and positions of peaks on $T(\beta, v)$ diagrams (filled circles) marked on the $\xi-\eta$ plane. The large open circles are positions of peaks on $T(\lambda, v)$ diagrams at $\beta=0'$.

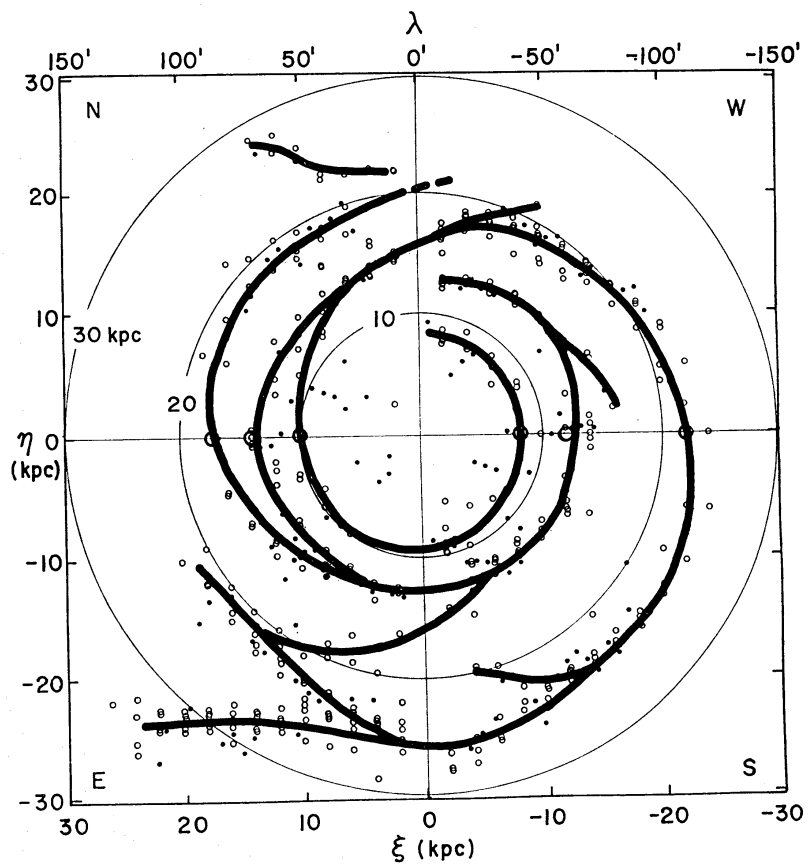

Fig. 10. Positions of arms traced on figure 9. Note a well developed trailing spiral arm at $R=20$–25 kpc in the western and southern quadrants. A grand design of two-armed spiral pattern is recognized when the arms at $R \gtrsim 15$ kpc are concerned.

As the original model spirals we take the bisymmetric, logarithmic spirals as used in the previous section (figure 4) and construct $T(\lambda, v)$ and $T(\beta, v)$ diagrams based on the model. Then we read a certain ridge position at a fixed longitude on the $T(\lambda, v)$ diagram and compare with the corresponding ridge position on the observed diagram at the same latitude (the nearest ridge to the calculated ridge position). If the two ridge positions (calculated and observed) agree with each other, we mark this position on the velocity field (figure 4) at the same longitude so that the ridge velocity coincides with the calculated velocity. If the ridge positions do not coincide, then we rotate the model spiral slightly without changing the other parameters and construct a new $T(\lambda, v)$ diagram for the rotated spiral. The rotation of the model spiral and construction of the $T(\lambda, v)$ diagrams are made iteratively until the calculated and observed ridge positions agree locally with each other. When they coincide, we mark the ridge position on the new velocity field corresponding to the finally rotated spiral density waves. In this way, we determine from point to point the arm positions on the galaxy plane. This procedure is applied to all the peak and ridge positions in the observed $T(\lambda, v)$ diagrams at various latitudes. A similar procedure is repeated using the $T(\beta, v)$ diagrams at various longitudes.

Figure 9 shows the arm positions thus marked on the plane of the galaxy as

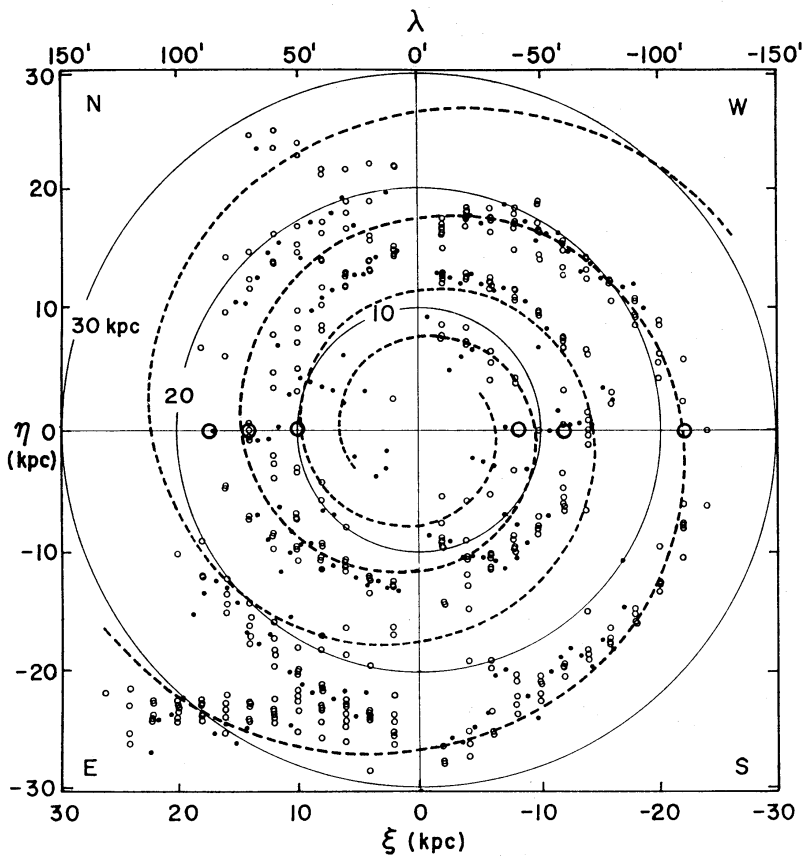

Fig. 11. Logarithmic bisymmetric spirals of pitch angle $\alpha=7^\circ.4$ superimopsed on figure 9 so that the SW arm at $R=20$–25 kpc fits one of the model spirals.

seen face on. Since the resolution of the beam is large compared with the observing intervals, an arm may appear on several neighboring diagrams at an identical position. Several marks representing one arm at a fixed longitude in figure 9 come from different diagrams. Therefore the spread of the marks in the figure does not imply a fine structure of an arm but represent the ambiguity in the determination of the arm position. Figure 10 shows the possible arm positions traced on figure 9. We find some definite arms which are located at $R\sim8$ to 30 kpc. The outermost arm in the SW side at $R=20$–25 kpc defines a well developed *trailing* spiral arm. In the inner region ($R\lesssim15$ kpc), the arms have rather a ring-like structure than a two-armed spiral pattern, although we find two clearly resolved arms at $R=8$ and 13 kpc in the SW side. In the NE side we find some spiral arms in the *trailing* sense: in particular, the eastern arm at $R\sim30$ kpc and the northern arm at $R\sim20$ kpc. In figure 11 we superpose two-armed logarithmic spirals with $\alpha=7^\circ.4$ on the presently obtained arm positions so that one of the spirals fits the outer arm position in the southern quadrant. The spirals are expressed with the following equation:

$$R=14.2\exp(-0.13\,\theta)\ \text{kpc}\,, \tag{8}$$

where θ is the position angle measured counterclockwise from the major axis.

The arm positions determined in figures 9 and 10 are in agreement with those obtained in Paper I using the velocity-to-space transformation method. Be-

cause we used here the positions of the ridges and peaks in the $T(\lambda, v)$ and $T(\beta, v)$ diagrams, the present result defines the positions of the arms more clearly than in Paper I. Furthermore the correction for the noncircular motion due to the density waves makes the present result more realistic. We note that the resulting arm positions in figure 9 are not affected by the initially taken spirals (figure 4), because we locally determined the arm positions by rotating the spirals.

5. Discussion

We have shown that the density-wave theory explains many characteristic features on the observed $T(\lambda, v)$ and $T(\beta, v)$ diagrams of M31. The main features are the wavy variation of the terminal velocity and the bifurcated distribution on the $T(\lambda, v)$ diagrams (figures 5 and 6), and the intensity peaks on the $T(\beta, v)$ diagrams which appear asymmetrically with respect to the line of $\beta=0'$ (figures 7 and 8). Similar features are well known in the $T(l, v)$ diagrams in our Galaxy (Burton 1971; Weaver 1974; Simonson 1976; Sawa 1978).

The bifurcated distribution on $T(\lambda, v)$ diagrams of M31 has been discussed by some authors. Cram et al. (1980) have proposed two possible explanations: the bifurcation is due to a warp all around the galaxy, or due to hydrogen gas at great heights above the central plane. Henderson (1979) has modeled $T(\lambda, v)$ diagrams based on the hypothesis of a thin, warped disk, showing that *at most two* bifurcated ridges appear on the diagrams. Byrd (1978) has shown that the tidal disturbance of the companion M32 can produce an off-plane distribution of the H I gas and possibly some velocity anomalies. However, it is unlikely that such off-plane debris of the H I gas produce a large-scale, systematic bifurcation on the $T(\lambda, v)$ diagrams. Comparing our calculated $T(\lambda, v)$ and $T(\beta, v)$ diagrams with the observed diagrams (figures 5–8), we can reasonably conclude that the bifurcation should be attributed to the spiral density waves in the M31 disk.

Many efforts have been devoted to derive spiral structure in M31, using optical constituents like H II regions, OB associations, and open clusters (Arp 1964; van den Bergh 1964; Simien et al. 1978; Hodge 1979). Most of these objects are concentrated in the inner region at $R \lesssim 15$ kpc, where their overall distributions are in agreement with the H I gas distributions obtained by Emerson (1974, 1976) and Unwin (1980a, b). Note that the H I maps obtained with the Cambridge interferometer (Unwin 1980b) cover only the inner region of $R \lesssim 15$ kpc. However, there have been controversial discussions on the spiral structure, whether it is trailing (e.g., Hodge 1979) or leading (Simien et al. 1978). In this respect our results as well as the H I-gas distribution obtained in Paper I give a clue to clarify the long-standing problem of the spiral structure. Namely, as shown in figures 9 and 10, M31 has a two-armed trailing spiral structure, in so far as the H I gas at $R \gtrsim 15$ kpc is concerned. An indication of the trailing outer spiral arm at $R \sim 20$–30 kpc in the southern quadrant has been also obtained by Whitehurst et al. (1978) under the assumption of circular rotation.

We draw further attention to an asymmetry in the appearance of the outermost spiral arms: the southern arm at $R=20$–25 kpc develops more prominently than the northern arm; the eastern arm at $R=30$ kpc seems to be extended from the southern arm at a larger pitch angle and reaches as far as ~ 35 kpc. This feature has been noticed by Whitehurst et al. (1978) as a perturbed off-plane outer arm. A similar asymmetric extension of an outer arm is obtained in M81

(van der Hulst 1979), which is thought to be produced by a tidal interaction with its companion, NGC 3077. In case of the M31 system, either M32 or NGC 205 could be a possible tidal disturber. However, M32 is located too close to the inner side (Byrd 1978) and NGC 205 is more likely to cause such a large-scale tidal asymmetry. An alternative possibility is that the eastern distant arm is a part of a bridge connecting M31 with an unseen companion or a massive object on its extension.

This work has been supported in part by the Scientific Research Fund of the Ministry of Education, Science, and Culture under Grant No. 574096 (T. Sawa in FY 1980) and No. 542003 (Y. Sofue in FY 1980 and 1981). The numerical computations were carried out on an OKITAC-DOS 50 at the Center for Educational Technology, Aichi University of Education.

References

Arp, H. 1964, *Astrophys. J.*, **139**, 1045.
Burton, W. B. 1971, *Astron. Astrophys.*, **10**, 76.
Burton, W. B. 1976, *Ann. Rev. Astron. Astrophys.*, 14, 275.
Byrd, G. G. 1978, *Astrophys. J.*, **226**, 70.
Cram, T.R., Roberts, M. S., and Whitehurst, R. N. 1980, *Astron. Astrophys. Suppl.*, **40**, 215.
Emerson, D. T. 1974, *Monthly Notices Roy. Astron. Soc.*, **169**, 607.
Emerson, D. T. 1976, *Monthly Notices Roy. Astron. Soc.*, **176**, 321.
Guibert, J. 1974, *Astron. Astrophys.*, **30**, 353.
Henderson, A. P. 1979, *Astron. Astrophys.*, **75**, 311.
Hodge, P. W. 1979, *Astron. J.*, **84**, 744.
Lin, C. C., Yuan, C., and Shu, F. H. 1969, *Astrophys. J.*, **155**, 721.
Sawa, T. 1978, *Astrophys. Space Sci.*, **53**, 467.
Simien, F., Athanassoula, E., Pellet, A., Monnet, G., Maucherat, A., and Courtès, G. 1978, *Astron. Astrophys.*, **67**, 73.
Simonson, S. C., III 1976, *Astron. Astrophys.*, **46**, 261.
Sofue, Y. and Kato, T. 1981, *Publ. Astron. Soc. Japan*, **33**, 449.
Unwin, S. C. 1980a, *Monthly Notices Roy. Astron. Soc.*, **190**, 551.
Unwin, S. C. 1980b, *Monthly Notices Roy. Astron. Soc.*, **192**, 243.
van den Bergh, S. 1964, *Astrophys. J. Suppl.*, **9**, 65.
van der Hulst, J.M. 1979, *Astron. Astrophys.*, **75**, 97.
Weaver, H. 1974, in *Galactic Radio Astronomy, IAU Symp. No. 60*, ed. F. J. Kerr and S. C. Simonson, III (Rediel Publ. Co., Dordrecht), p. 573.
Whitehurst, R. N., Roberts, M. S. and Cram, T. R. 1978, in *Structure and Properties of Nearby Galaxies, IAU Symp. No. 77*, ed. E. M. Berkhuijsen and R. Wielebinski (Reidel Publ. Co., Dordrecht), p. 175.
Yuan, C. 1969, *Astrophys. J.*, **158**, 889.